Available online at www.sciencedirect.com
ScienceDirect
Bioorganic & Medicinal Chemistry Letters 17 (2007) 200–204
Bioorganic & Medicinal Chemistry Letters

Syntheses of F-18 labeled fluoroalkyltyrosine derivatives and their biological evaluation in rat bearing 9L tumor

Byung Seok Moon,[a,c] Tae Sup Lee,[b] Kyo Chul Lee,[a] Gwang Il An,[a] Gi Jeong Cheon,[a,b] Sang Moo Lim,[b] Chang Woon Choi,[b] Dae Yoon Chi[c] and Kwon Soo Chun[a,*]

[a]*Laboratory of Radiopharmaceuticals, Korea Institute of Radiological and Medical Sciences, 215-4 Gongneungdong, Nowongu, Seoul 139-706, Republic of Korea*
[b]*Laboratory of Nuclear Medicine, Korea Institute of Radiological and Medical Sciences, 215-4 Gongneungdong, Nowongu, Seoul 139-706, Republic of Korea*
[c]*Department of Chemistry, Inha University, 253 Yonghyundong, Namgu, Inchon 402-751, Republic of Korea*

Received 1 August 2006; revised 19 September 2006; accepted 21 September 2006
Available online 10 October 2006

Abstract—We hereby report the synthesis of four fluorine-18 labeled tyrosine derivatives, 3-(2-[^{18}F]fluoroethyl)tyrosine ([^{18}F]**1**, [^{18}F]*ortho*-FET), 3-(3-[^{18}F]fluoropropyl)tyrosine ([^{18}F]**2**, [^{18}F]*ortho*-FPT) *O*-methyl-[3-(2-[^{18}F]fluoroethyl)]tyrosine ([^{18}F]**3**, [^{18}F]MFET), and *O*-methyl-[3-(3-[^{18}F]fluoropropyl)]tyrosine ([^{18}F]**4**, [^{18}F]MFPT). The fluorine-18 labeled tyrosine derivatives were prepared by the displacement reaction of the ethyl and propyl tosylates with K[^{18}F]/K2.2.2 in acetonitrile under no-carrier-added (NCA) conditions, followed by hydrolysis with 4 N HCl. The biological properties of labeled compounds were evaluated in rats bearing 9L tumor after an intravenous injection and PET image was obtained. The tumor/blood and tumor/brain ratios were 2.06, 2.92 for [^{18}F]**1**, 2.25, 4.05 for [^{18}F]**2**, 2.88, 1.90 for [^{18}F]**3**, and 2.00, 2.60 for [^{18}F]**4** at 60 min post injection, respectively. The PET image showed localized accumulation of PET tracers in 9L glioma of the rat.

Of all nuclear medicine imaging modalities, positron emission tomography (PET) offers the highest resolution and allows the tracer concentration in tissues to be quantified.[1] One of the PET tracers, 2-[^{18}F]fluorodeoxyglucose (FDG) as a parameter of the glucose metabolism, has been used widely in PET for oncology, neurology, and psychiatry, as well as for treatment evaluation.[2] However, [^{18}F]FDG images of solid tumors are often complicated by the high uptake in both the tumor and nonmalignant, inflammatory tissue. Therefore, so far, there has been considerable research into the development of new oncologic PET tracers.[3] For more than 40 years, labeled amino acids such as [^{11}C-*methyl*]methionine (MET),[4] 3-[^{18}F]fluoro-α-methyltyrosine (FMT),[5] [^{18}F]fluoro-L-phenylalanine,[6] 1-amino-3-[^{18}F]fluorocyclobutane-1-carboxylic acid,[7] [^{18}F]fluoro-L-proline,[8] [^{11}C-*methyl*]-α-aminoisobutyric acid,[9] 4-borono-2-[^{18}F]fluoro-L-phenylalanine (FBPA),[10] and L-3-[^{123}I]iodo-α-methyltyrosine[11] have been developed and evaluated for their potential use in oncology, particularly for tumors of the brain, lung, and breast. In general, radiolabeled amino acids can be categorized in two—natural and non-natural amino acids analogues labeled with various radionuclides.[12] Radiolabeled natural amino acid analogues have been extensively investigated for humans to detect tumors such as brain and systemic tumors. However, they are readily metabolized through multiple pathways, giving rise to several radioactive metabolites. Such susceptibility makes pharmacokinetic study in living substances hard to be obtained for given time period. On the other hand, radiolabeled non-natural amino acid analogues provide some considerable advantages. As they are slowly or differently metabolized, the pharmacokinetic analysis after post injection of radiotracers becomes quite simple. Therefore, recent efforts have focused on the development of radiolabeled non-natural amino acids.

Recently, among new structurally similar amino acid analogues, *O*-(2-[^{18}F]fluoroethyl)-L-tyrosine ([^{18}F]FET),[13,14] *O*-(3-[^{18}F]fluoropropyl)-L-tyrosine ([^{18}F]FPT)[15] have

Keywords: Amino acids; *O*-(2-[^{18}F]Fluoroethyl)-L-tyrosine (L-[^{18}F]FET); Labeled tyrosine; Tumor imaging; PET.
* Corresponding author. Tel.: +82 2 970 1337; fax: +82 2 970 2409; e-mail: kschun@kcch.re.kr

0960-894X/$ - see front matter © 2006 Elsevier Ltd. All rights reserved.
doi:10.1016/j.bmcl.2006.09.063

been developed and evaluated. [^{18}F]FET has a low uptake in activated inflammatory cells in an experimental acute abscess model and in inflammation within lymph nodes.[16,17] [^{18}F]FPT is superior to FDG and has a slight advantage over FET in being able to differentiate a tumor from inflammation, and like [^{18}F]FET, it appears to be a potential amino acid tracer for tumor imaging with PET.[15]

Radiopharmaceuticals labeled with fluorine-18 are being used increasingly in clinical diagnoses. Although fluorine-18 is the most attractive radionuclide for the preparation of imaging agents for PET, the labeling of amino acids with fluorine-18 is often difficult, particularly in aromatic positions. An alternative way of labeling aromatic systems with fluorine-18 involves the introduction of a fluoroalkyl group to an aromatic position, rather than by direct labeling with a fluorine atom.[18] Lee et al. reported the in vitro biological stability of fluoroalkyl groups, such as fluoromethyl, fluoroethyl, and fluoropropyl, using rat hepatic microsomes and human serum.[19] In the current study, fluoroethyl and fluoropropyl groups were introduced at the R1 position and OCH3 was introduced at the R2 position. The main reason for fluoroalkyl groups in R1 position is just synthetically easy on introduce the fluoroalkyl group at R1 position which is *ortho*-position of phenol. And if we protected phenol by methylation, the compounds **3** and **4** would be more lipophilic than the corresponding compounds **1** and **2** with a similar effect to FET (Fig. 1). We report the synthesis and biological evaluation of four novel non-natural fluorine-substituted tyrosine derivatives for tumor imaging, 3-(2-[^{18}F]fluoroethyl)tyrosine ([^{18}F]**1**, [^{18}F]*ortho*-FET), 3-(3-[^{18}F]fluoropropyl)tyrosine ([^{18}F]**2**, [^{18}F]*ortho*-FPT), *O*-methyl[3-(2-[^{18}F]fluoroethyl)]tyrosine ([^{18}F]**3**, [^{18}F]MFET), and *O*-methyl[3-(3-[^{18}F]fluoropropyl)]tyrosine ([^{18}F]**4**, [^{18}F]MFPT). The biological properties of these new radiotracers were evaluated using in vivo uptake assays in rats bearing 9L (glioma) and PET image.

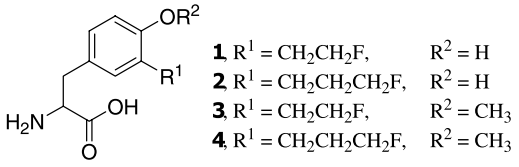

Figure 1. Structure of the tyrosine derivatives used in this study.

The precursors for **1** (*ortho*-FET), **2** (*ortho*-FPT), **3** (MFET), and **4** (MFPT) were prepared in six steps from 3-iodotyrosine (**5**) as shown in Scheme 1. 3-Iodotyrosine methyl ester (**6**) was synthesized by the reaction with 3.0 equiv of trimethylsilyl chloride (TMSCl) in MeOH at rt for 24 h, followed by removal of TMSCl and MeOH by evaporation and isolation by flash column chromatography. *N*-(*tert*-butoxycarbonyl)-3-iodo-L-tyrosine methyl ester (**7**) was prepared by the reaction of $(Boc)_2O$ with triethylamine (TEA) at rt for 2 h in 70% yield. MOM protected *N*-(*tert*-butoxycarbonyl)-3-iodo-L-tyrosine methyl ester (**8a**) was synthesized using MOMCl and NaH in dry THF at 0–70 °C for 1 h in 65% yield. Introduction of methyl moiety (**8b**) was obtained through a reaction with CH_3I and K_2CO_3 in DMSO at rt for 2 h in 75% yield. Treatment of the R group-protected **8a** or **8b** with allyl (or vinyl) tributylstannane and $Pd(PPh_3)_4$ in anhydrous 1,4-dioxane at 90 °C for 1 h afforded the R group induced 3-allyl (or vinyl) tyrosine **9a**–**9d** in 50–60% yields. Hydroboration of alkenes **9a**–**9d** using a borane–THF complex in THF at 0 °C for 2 h and subsequent oxidation with alkaline peroxide gave the aliphatic alcohols **10a**–**10d** in 45–60% yields. The tosylation of the alcohol afforded the tosylates **11a**–**11d** in 75–85% yields. The authentic compounds **1**, **2**, **3**, and **4** were synthesized from the tosylated compounds using TBAF·3H$_2$O followed by deprotection of MOM and Boc groups with 4 N HCl and then purified with reverse-phase semi-HPLC (see a Ref. 20: structure analysis data).

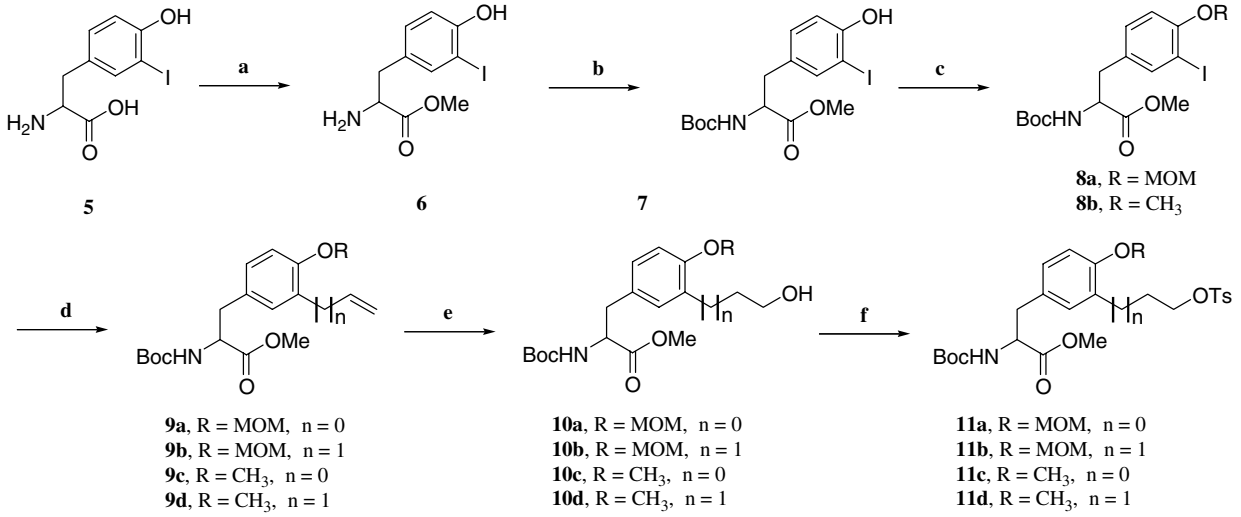

Scheme 1. Reagents and conditions: (a) TMSCl, MeOH, rt, 24 h, 75%; (b) $(Boc)_2O$, TEA, MeOH, rt, 2 h, 70%; (c) NaH, MOMCl, THF, 0–70 °C, 1 h, 65% for R = MOM; CH_3I, K_2CO_3, DMSO, rt, 2 h, 75% for R = CH_3; (d) allyl (or vinyl) tributylstannane, $Pd(PPh_3)_4$, 1,4-dioxane, 90 °C, 1 h, 50–60%; (e) i—BH_3–THF complex, THF, 0 °C, 2 h, ii—4 N NaOH, 30% H_2O_2, 45–60%; (f) TsCl, TEA, CH_2Cl_2, rt, 2 h, 75–85%.

The F-18 labeled tyrosine derivatives were prepared by the nucleophilic substitution of the precursors (**11a**–**11d**) with the fluoride–Kryptofix 2.2.2. complex (37.0 GBq) in acetonitrile (1.0 mL) at 90 °C for 20 min followed by hydrolysis with 4 N HCl at 110 °C for 20 min in open conditions. The labeled compounds were separated by HPLC using a reverse semi-preparative column: Hibar® EtOH/H_2O/AcOH = 100:875:25, 2.5 g NH_4OAc/L, flow rate: 2.0 mL/min for [^{18}F]**1** (t_R: 14–15 min) and [^{18}F]**2** (t_R: 21–23 min); EtOH/H_2O/AcOH = 200:775:25, 2.5 g NH_4OAc/L, flow rate: 3.0 mL/min for [^{18}F]**3** (t_R: 15–17 min) and [^{18}F]**4** (t_R: 19–22 min). Further purification was carried out through a strong cation exchange resin and the pure compounds [^{18}F]**1**, [^{18}F]**2**, [^{18}F]**3**, and [^{18}F]**4** were collected with a phosphate-buffered solution (9.0 mL, pH 7.4) and 8.4% sodium bicarbonate solution (2.5 mL) mixture. Quality control was performed by HPLC [LiChrosorb RP-18, 250 × 4 mm and chiral column (Crownpak CR (+), 150 × 4 mm)]. The decay-corrected radiochemical yield for [^{18}F]**1**, [^{18}F]**2**, [^{18}F]**3**, and [^{18}F]**4** was approximately 15%, 45%, 24%, and 48% after HPLC purification, respectively. The radiochemical purity was >95%. The specific activity was >37.0 GBq/μmol for [^{18}F]**2**, [^{18}F]**3**, and [^{18}F]**4**, and 11.0 ± 2.4 GBq/μmol for [^{18}F]**1** in a synthesis time of approximately 100 min. The total elapsed times needed to prepare the [^{18}F]fluorotyrosine derivatives were about 110 min.

The ratio of D- and L-[^{18}F]fluoroalkyltyrosine was checked using chiral column: Daicel, Crownpak CR (+), 150 × 4.0 mm, 5% MeOH/H_2O (pH 2.0, $HClO_4$), flow rate: 0.8 mL/min, HPLC system as D-[^{18}F]fluoroalkyltyrosine derivatives: 17–26% and L-[^{18}F]fluoroalkyltyrosine derivatives: 74–83% (n = 2 or 3). One chiral HPLC diagram of M[^{18}F]FPT as an example is shown in Figure 2.

The partition coefficients of the [^{18}F]fluoroalkyltyrosine moieties were measured using 2.0 mL 1-octanol as the organic phase and 2.0 mL water phase. After HPLC purification, 10 μL of each radioactive sample was added and mixed for 2 min at room temperature. The radioactivity of 300 μL of each phase was measured. The log P of the [^{18}F]fluoroalkyltyrosine derivatives **1**, **2**, **3**, and **4** were −1.37, −1.07, −0.75, and −0.29, respectively.

The biodistribution studies and tumor uptake were investigated in Fisher 344 rats bearing 9L tumor. The experimental procedures were performed 14–18 days after inoculating the rats with 5×10^6 tumor cells. Before applying the radiotracer, the animals were anesthetized with ethyl ether. Subsequently, an approximately 3.7 MBq/100 μL phosphate-buffered saline solution of [^{18}F]fluoroalkyltyrosine was injected into the tail vein. The animals were sacrificed by ethyl ether at various times and the organs of interest were rapidly dissected. The radioactivity in the weighed tissue samples was measured using a gamma counter. The data are expressed as the percentage of injected dose per gram of tissue (n = 4). Each reported value represents mean and standard deviation. [^{18}F]Fluoroalkyltyrosine derivatives were tested for statistical significance using one-way ANOVA. p values <0.05 were considered significant.

The biodistribution data of [^{18}F]fluoroalkyltyrosines [^{18}F]**1**, [^{18}F]**2**, [^{18}F]**3**, and [^{18}F]**4** in rats with 9L glioma are summarized in Tables 1–4, respectively. The data present as percentage of injected dose per gram of tissues (%ID/g).

In the [^{18}F]*ortho*-FET biodistribution, all organs showed the rapid distribution of the tracer, which was completed in less than 10 min post-injection and had decreased by 120 min. The femur uptake was significantly higher than that of the other organs. The reason [^{18}F]*ortho*-FET

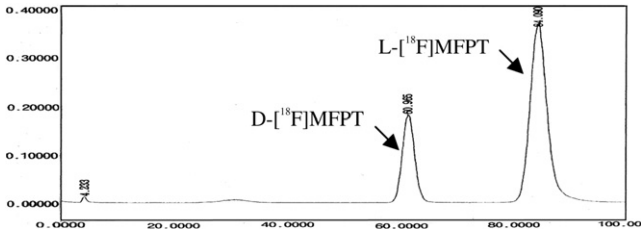

Figure 2. The ratio of D-form M[^{18}F]FPT (t_R = 61 min) and L-form M[^{18}F]FPT (t_R = 84 min).

Table 1. Biodistribution data of [^{18}F]*ortho*-FET ([^{18}F]**1**) in rats bearing 9L tumor

Organ	Time point (min)			
	10	30	60	120
Blood	0.34 ± 0.06	0.13 ± 0.06	0.06 ± 0.01	0.08 ± 0.03
Liver	0.35 ± 0.06	0.13 ± 0.04	0.07 ± 0.01	0.07 ± 0.04
Lung	0.30 ± 0.04	0.12 ± 0.04	0.07 ± 0.01	0.07 ± 0.04
Kidney	0.80 ± 0.14	0.23 ± 0.05	0.13 ± 0.03	0.14 ± 0.07
Intestine	0.42 ± 0.08	0.21 ± 0.09	0.15 ± 0.07	0.13 ± 0.06
Femur	0.88 ± 0.05	0.77 ± 0.23	0.76 ± 0.06	0.46 ± 0.37
Pancreas	0.41 ± 0.04	0.17 ± 0.04	0.12 ± 0.08	0.09 ± 0.06
Muscle	0.17 ± 0.02	0.11 ± 0.03	0.07 ± 0.02	0.06 ± 0.04
Brain	0.08 ± 0.01	0.05 ± 0.00	0.04 ± 0.01	0.03 ± 0.03
Tumor	0.34 ± 0.04	0.17 ± 0.01	0.12 ± 0.03	0.09 ± 0.07

(Number of rats/group; n = 4. Data represent as means ± SD).

Table 2. Biodistribution data of [^{18}F]*ortho*-FPT ([^{18}F]**2**) in rats bearing 9L tumor

Organ	Time point (min)			
	10	30	60	120
Blood	1.05 ± 0.09	0.81 ± 0.07	0.64 ± 0.10	0.50 ± 0.05
Liver	1.26 ± 0.11	0.95 ± 0.07	0.73 ± 0.12	0.55 ± 0.05
Lung	0.98 ± 0.10	0.78 ± 0.08	0.61 ± 0.10	0.45 ± 0.05
Kidney	1.84 ± 0.12	1.20 ± 0.20	0.83 ± 0.13	0.60 ± 0.09
Intestine	0.97 ± 0.36	1.00 ± 0.08	0.62 ± 0.13	0.51 ± 0.22
Femur	0.72 ± 0.12	1.06 ± 0.04	1.45 ± 0.26	0.99 ± 0.16
Pancreas	2.20 ± 0.32	1.77 ± 0.51	1.56 ± 0.22	1.58 ± 0.07
Muscle	0.72 ± 0.10	0.73 ± 0.08	0.59 ± 0.08	0.54 ± 0.06
Brain	0.21 ± 0.03	0.32 ± 0.03	0.35 ± 0.06	0.22 ± 0.02
Tumor	1.04 ± 0.24	1.13 ± 0.26	1.41 ± 0.33	0.79 ± 0.48

(Number of rats/group; n = 4. Data represent as means ± SD).

Table 3. Biodistribution data of [^{18}F]MFET ([^{18}F]**3**) in rats bearing 9L tumor

Organ	Time point (min)			
	10	30	60	120
Blood	0.45 ± 0.03	0.41 ± 0.05	0.25 ± 0.03	0.29 ± 0.04
Liver	0.55 ± 0.04	0.40 ± 0.04	0.36 ± 0.08	0.39 ± 0.02
Lung	0.47 ± 0.03	0.37 ± 0.04	0.37 ± 0.13	0.35 ± 0.01
Kidney	1.07 ± 0.15	0.64 ± 0.12	0.52 ± 0.05	0.53 ± 0.09
Intestine	0.40 ± 0.11	0.34 ± 0.05	0.33 ± 0.12	0.39 ± 0.04
Femur	0.29 ± 0.05	0.25 ± 0.05	0.22 ± 0.05	0.25 ± 0.02
Pancreas	1.38 ± 0.89	1.33 ± 0.43	1.43 ± 0.56	1.56 ± 0.64
Muscle	0.40 ± 0.03	0.40 ± 0.03	0.42 ± 0.09	0.44 ± 0.05
Brain	0.32 ± 0.04	0.34 ± 0.04	0.39 ± 0.12	0.57 ± 0.43
Tumor	0.71 ± 0.10	0.64 ± 0.08	0.74 ± 0.25	0.78 ± 0.06

(Number of rats/group; $n = 4$. Data represent as means ± SD).

Table 4. Biodistribution data of [^{18}F]MFPT ([^{18}F]**4**) in rats bearing 9L tumor

Organ	Time point (min)			
	10	30	60	120
Blood	0.76 ± 0.19	0.32 ± 0.05	0.24 ± 0.07	0.12 ± 0.03
Liver	0.87 ± 0.22	0.37 ± 0.05	0.28 ± 0.07	0.17 ± 0.09
Lung	0.81 ± 0.20	0.34 ± 0.04	0.28 ± 0.13	0.14 ± 0.03
Kidney	4.61 ± 0.69	1.60 ± 0.27	1.21 ± 0.20	0.66 ± 0.11
Intestine	0.78 ± 0.07	0.44 ± 0.12	0.26 ± 0.09	0.15 ± 0.06
Femur	0.50 ± 0.14	0.25 ± 0.02	0.18 ± 0.05	0.09 ± 0.01
Pancreas	1.57 ± 0.53	0.74 ± 0.16	0.56 ± 0.27	0.31 ± 0.06
Muscle	0.70 ± 0.19	0.36 ± 0.16	0.31 ± 0.12	0.14 ± 0.02
Brain	0.38 ± 0.15	0.26 ± 0.03	0.19 ± 0.06	0.08 ± 0.02
Tumor	1.07 ± 0.25	0.72 ± 0.17	0.47 ± 0.15	0.31 ± 0.22

(Number of rats/group; $n = 4$. Data represent as means ± SD).

([^{18}F]**1**) is unstable in vivo due to defluorination by elimination, uptake of most organs was decreased as a time elapsed. The tumor-to-blood (T/Bl) uptake ratio 60 min after injection of [^{18}F]**1** was 2.06 ± 0.25, while the tumor-to-brain (T/Br) ratio was 2.92 ± 0.41.

The organ uptake of [^{18}F]*ortho*-FPT ([^{18}F]**2**) decreased in a time-dependent manner except for the femur, brain, and tumor, which showed the retention of the tracer. The highest uptake in tumor was reached at 60 min after injection. The tumor uptake was higher than that of the liver, kidney, and lung at 60 min. The uptake of [^{18}F]*ortho*-FPT in the tumor of 9L bearing rat reached approximately 1.04 ± 0.24 %ID/g at 10 min after injection and increased to 1.41 ± 0.33 %ID/g at 60 min after injection. The T/Bl and T/Br uptake ratios were 2.25 ± 0.25 and 4.05 ± 1.14 at 60 min after injection, respectively.

The [^{18}F]MFET ([^{18}F]**3**) tracer showed the highest uptake in the pancreas and there was only a slight difference between most organs in terms of the activity retained in the tissues during experimental time.

The tumor and brain uptake slightly increased with time elapsed. The T/Bl and T/Br uptake ratios were 2.88 ± 0.59 and 1.90 ± 0.39 at 60 min after injection, respectively.

In the biodistribution data of [^{18}F]MFPT ([^{18}F]**4**), the initial level of accumulation of radioactivity in all tissues after injection was high and rapidly decreased between 10 and 30 min. At 10 min, the radioactivity of [^{18}F]**4** was greater in the kidney than in all other organs. The tumor uptake of [^{18}F]**4** peaked at 10 min (1.07 ± 0.25 %ID/g) and decreased to 0.31 ± 0.22 %ID/g by 120 min (decreased 3.45 times of initial uptake). The uptake in blood and brain also decreased in a time-dependent manner with the rate of decrease being 4.75 and 6.33 times. The T/Bl and T/Br uptake ratios were 2.00 ± 0.47 and 2.60 ± 0.52 at 60 min after injection, respectively.

PET images of the [^{18}F]*ortho*-FPT and [^{18}F]MFET ([^{18}F]**3**) in rat bearing 9L tumor are shown in Figure 3. PET image acquisition was performed in rat with 9L tumor on the right or left thigh. The rat was used in the PET experiment when the tumor size had grown to approximately 985 ± 402 mm.[3] After 60 min of intravenous injection of radiotracers (37.0 MBq), rats were sacrificed with lethal dose of ethyl ether. Using dedicated PET scanner (ECAT EXACT HR+ scanner, SIEMENS/CTIMI, Knoxville, Tenn), acquisition was performed in 2-dimensional mode. Using a germanium-68 source, transmission images were obtained for 5 min to correct for photon attenuation. After the transmission scan, emission images were obtained for 15 min, and acquisition data were reconstructed using iterative reconstruction and segmented attenuation. The total acquisition time was 20 min. [^{18}F]*ortho*-FPT ([^{18}F]**2**) and [^{18}F]MFET ([^{18}F]**3**) were selectively accumulated in 9L tumor of Fisher 344 rat. [^{18}F]*ortho*-FPT ([^{18}F]**2**) accumulation in all tissues was low except for pancreas and kidney. [^{18}F]MFET uptake was high in pancreas, but radioactivity of other tissues was low.

In biodistribution studies, the %ID/g in the blood of the rats injected with [^{18}F]**1**–**4** decreased from 10 min post-injection to 120 min post-injection. Compounds [^{18}F]**2** and [^{18}F]**4** showed faster blood clearance than [^{18}F]**1** and [^{18}F]**3**. The uptake of [^{18}F]**1**, [^{18}F]**2**, and [^{18}F]**4** in pancreas decreased in a time-dependent manner, but the uptake of [^{18}F]**3** increased. In tumor and brain, the

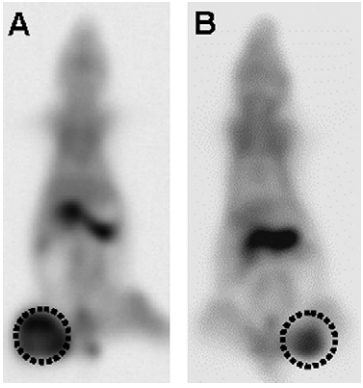

Figure 3. [^{18}F]*ortho*-FPT (A) and [^{18}F]MFET (B) PET image in rat bearing 9L tumor at 60 min post-injection. (A) 9L tumor is in right thigh of rat. (B) 9L tumor is in left thigh of rat.

uptakes of [^{18}F]**2** and [^{18}F]**3** increased with time elapsed but the uptake of [^{18}F]**1** and [^{18}F]**4** decreased. On the basis of these results, the ratios of tumor-to-blood (T/B) and tumor-to-brain (T/Br) for radiotracers were compared with [^{18}F]FET (T/Bl ratio: 1.80 ± 0.13; T/Br ratio: 2.81 ± 0.24).[21] The T/Bl ratios of [^{18}F]**1**, [^{18}F]**2**, and [^{18}F]**4** were similar to that of [^{18}F]FET. However, the T/Bl ratio of [^{18}F]**3** was higher than that of [^{18}F]FET at 60 min post-injection ($p < 0.05$). The T/Br ratio of [^{18}F]**2** was higher than that of [^{18}F]FET ($p < 0.05$). The T/Br ratios of [^{18}F]**1**, [^{18}F]**3**, and [^{18}F]**4** were similar to that of [^{18}F]FET. These results demonstrate that [^{18}F]*ortho*-FPT ([^{18}F]**2**) showed similar T/Bl ratio with [^{18}F]FET and better T/Br ratios in 9L tumor bearing rat than [^{18}F]FET. [^{18}F]MFET ([^{18}F]**3**) showed better T/Bl ratio than [^{18}F]FET and similar T/Br ratios than [^{18}F]FET. In the PET study of the brain tumor, the image contrast of [^{18}F]fluoroalkyltyrosines appears to be similar to that of [^{18}F]FET (data not shown). Moreover, [^{18}F]fluoroalkyltyrosine can be efficiently radiolabeled with F-18. Therefore, it is expected that [^{18}F]*ortho*-FPT ([^{18}F]**2**) may have potential application in the detection of brain tumors and [^{18}F]MFET may have some advantage in peripheral tumor imaging. In conclusion, [^{18}F]*ortho*-FPT ([^{18}F]**2**) and [^{18}F]MFET ([^{18}F]**3**) might show a possibility to use a more useful tumor imaging agent than [^{18}F]FET.

Acknowledgments

This study was supported by Korea Science and Engineering Foundation (KOSEF) and Ministry of Science & Technology (MOST), Republic of Korea, through its National Nuclear Technology Program. Thanks to Kwang Sun Woo and Wee Sup Jung for technical assistance.

References and notes

1. *Clinical positron emission tomography*; Hubner, K. F., Collmann, J., Buonocore, E., Kabalka, G. W., Eds.; Mosby: St. Louis, MO, 1991; p 110.
2. Tang, G. H. *Acta Pharm. Sin.* **2001**, *36*, 470.
3. Laverman, P.; Boerman, O. C.; Corstens, F. H. M.; Oyen, W. J. *Eur. J. Nucl. Med.* **2002**, *29*, 681.
4. Langstrom, B.; Antoni, G.; Gullberg, P.; Halldin, C.; Malmborg, P.; Nagren, K.; Rimland, A.; Svard, H. *J. Nucl. Med.* **1987**, *28*, 1037.
5. Inoue, T.; Tomiyoshi, K.; Higuichi, T.; Ahmed, K.; Sarwar, M.; Aoyagi, K.; Amano, S.; Alyafei, S.; Zhang, H. N.; Endo, K. *J. Nucl. Med.* **1998**, *39*, 663.
6. Kubota, K.; Ishiwata, K.; Kubota, R.; Yamada, S.; Takahashi, J.; Abe, Y.; Fukuda, H.; Ido, T. *J. Nucl. Med.* **1996**, *37*, 320.
7. Shoup, T. M.; Olson, J.; Hoffman, J. M.; Votaw, J.; Eshima, D.; Eshima, L.; Camp, V. M.; Stabin, M.; Votaw, D.; Goodman, M. M. *J. Nucl. Med.* **1999**, *40*, 331.
8. Wester, H. J.; Herz, M.; Senekowitsch-Schmidtke, R.; Schwaiger, M.; Stocklin, G.; Hamacher, K. *Nucl. Med. Biol.* **1999**, *26*, 259.
9. Bading, J. R.; Kan-Mitchell, J.; Conti, P. S. *Nucl. Med. Biol.* **1996**, *23*, 779.
10. Ishiwata, K.; Ido, T.; Mejia, A. A.; Ichihashi, M.; Mishima, Y. *Appl. Radiat. Isot.* **1991**, *42*, 325.
11. Langen, K. J.; Coenen, H. H.; Roosen, N.; Kling, P.; Muzik, O.; Herzog, H.; Kuwert, T.; Stocklin, G.; Feinendegen, L. E. *J. Nucl. Med.* **1990**, *31*, 281.
12. Martarello, L.; McConathy, J.; Camp, V. M.; Malveaux, E. J.; Simpson, N. E.; Simpson, C. P.; Olson, J. J.; Bowers, G. D.; Goodman, M. M. *J. Med. Chem.* **2002**, *45*, 2250.
13. Wester, H. J.; Herz, M.; Weber, W.; Heiss, P.; Senekowitsch-Schmidtke, R.; Schwaiger, M.; Stocklin, G. *J. Nucl. Med.* **1999**, *40*, 205.
14. Heiss, P.; Mayer, S.; Herz, M.; Wester, H. J.; Schwaiger, M.; Senekowitsch-Schmidtke, R. *J. Nucl. Med.* **1999**, *40*, 1367.
15. Tang, G. H.; Wang, M. F.; Tang, X. L.; Luo, L.; Gan, M. Q. *Nucl. Med. Biol.* **2003**, *30*, 733.
16. Kaim, A. H.; Weber, B.; Kurrer, M. O.; Westera, G.; Schweitzer, A.; Gottschalk, J.; von Schulthess, G. K.; Buck, A. *Eur. J. Nucl. Med.* **2002**, *29*, 648.
17. Rau, F. C.; Weber, W. A.; Wester, H. J.; Herz, M.; Becker, I.; Kruger, A.; Schwaiger, M.; Senekowitsch-Schmidtke, R. *Eur. J. Nucl. Med.* **2002**, *29*, 1039.
18. (a) Choe, Y. S.; Song, D. H.; Lee, K.-J.; Kim, S. E.; Choi, Y.; Lee, K. H.; Kim, B.-T.; Oh, S. J.; Chi, D. Y. *Appl. Radiat. Isot.* **1998**, *49*, 73; (b) Barrio, J. R.; Petric, A.; Satyamurthy, N.; Huang, S. C.; Yu, D. C. *J. Nucl. Med.* **1994**, *35S*, 83P.
19. Lee, K. C.; Lee, S. Y.; Choe, Y. S.; Chi, D. Y. *Bull. Korean Chem. Soc.* **2004**, *25*, 1225.
20. Structure analysis data. *ortho*-FET (**1**): ^{1}H NMR (300 MHz, CD_3OD) δ 7.07 (s, 1H), 7.02 (dd, $J = 8.1$, 2.2 Hz, 1H), 6.77 (d, $J = 8.1$ Hz, 1H), 4.67 (dt, $J = 47.4$, 6.9 Hz, 2H), 3.72 (t, $J = 4.5$ Hz, 1H), 3.19–3.17 (m, 1H), 3.04–2.92 (m, 3H); MS (FAB) *m*/*z*: 228 (MH^+). HRMS (FAB) Calcd for $C_{11}H_{15}NO_3F$ (MH^+) 228.1036. Found: 228.1036. *ortho*-FPT (**2**): ^{1}H NMR (300 MHz, CD_3OD) δ 7.05 (d, $J = 1.8$ Hz, 1H), 6.99 (dd, $J = 8.1$, 2.4 Hz, 1H), 6.76 (d, $J = 1$H), 4.46 (dt, $J = 47.4$, 6.3 Hz, 2H), 3.74–3.71 (m, 1H), 3.20–3.18 (m, 1H), 2.96–2.93 (m, 1H), 2.70 (t, $J = 7.5$ Hz, 2H), 2.04–1.88 (m, 2H); MS (FAB) *m*/*z*: 242 (MH^+). HRMS (FAB) Calcd for $C_{12}H_{17}NO_3F$ (MH^+) 242.1192. Found: 242.1189. MFET (**3**): ^{1}H NMR (300 MHz, CD_3OD) δ 7.20–7.14 (m, 1H), 6.93 (d, $J = 8.1$ Hz, 1H), 4.56 (dt, $J = 47.4$, 6.6 Hz, 2H), 3.83 (s, 3H), 3.76–3.72 (m, 1H), 3.27–3.22 (m, 1H), 3.06–2.95 (m, 3H); MS (FAB) *m*/*z*: 242 (MH^+). HRMS (FAB) Calcd for $C_{12}H_{17}NO_3F$ (MH^+) 242.1192. Found: 242.1192. MFPT (**4**): ^{1}H NMR (300 MHz, CD_3OD) δ 7.15–7.11 (m, 2H), 6.91 (d, $J = 8.1$ Hz, 1H), 4.44 (dt, $J = 47.4$, 6.3 Hz, 2H), 3.82 (s, 3H), 3.75–3.72 (m, 1H), 3.24–3.22 (m, 1H), 2.95–2.92 (m, 1H), 2.68 (t, $J = 7.5$ Hz, 2H), 2.02–1.93 (m, 2H); MS (FAB) *m*/*z*: 256 (MH^+). HRMS (FAB) Calcd for $C_{13}H_{19}NO_3F$ (MH^+) 256.1349. Found: 256.1349.
21. Moon, B. S.; Kim, S. W.; Lee, T. S.; Ahn, S. H.; Lee, K. C.; An, G. I.; Yang, S. D.; Chi, D. Y.; Choi, C. W.; Lim, S. M.; Chun, K. S. *Bull. Korean Chem. Soc.* **2005**, *26*, 91.